2017

Femtosecond Laser Induced Structural Dynamics and Melting of Cu (111) Single Crystal. An Ultrafast Time-Resolved X-Ray Diffraction Study

Runze Li

Omar A. Ashour

Jie Chen

H. E. Elsayed-Ali
Old Dominion University, helsayed@odu.edu

Peter M. Rentzepis

Follow this and additional works at: https://digitalcommons.odu.edu/ece_fac_pubs

Part of the Condensed Matter Physics Commons

Femtosecond laser induced structural dynamics and melting of Cu (111) single crystal. An ultrafast time-resolved x-ray diffraction study

Runze Li,[1] Omar A. Ashour,[1] Jie Chen,[2] H. E. Elsayed-Ali,[3] and Peter M. Rentzepis[1,a)]

[1]*Department of Electrical and Computer Engineering, Texas A&M University, College Station, Texas 77843, USA*
[2]*Key Laboratory for Laser Plasmas (Ministry of Education), Department of Physics and Astronomy and IFSA Collaborative Innovation Center, Shanghai Jiao Tong University, Shanghai 200240, China*
[3]*Department of Electrical and Computer Engineering, Old Dominion University, Norfolk, Virginia 23529, USA*

Femtosecond, 8.04 keV x-ray pulses are used to probe the lattice dynamics of a 150 nm Cu (111) single crystal on a mica substrate irradiated with 400 nm, 100 fs laser pulses. For pump fluences below the damage and melting thresholds, we observed lattice contraction due to the formation of a blast force and coherent acoustic phonons with a period of ~69 ps. At larger pump fluence, solid to liquid phase transition, annealing, and recrystallization were measured in real time by monitoring the intensity evolution of the probing fs x-ray rocking curves, which agreed well with theoretical simulation results. The experimental data suggest that the melting process is a purely thermal phase transition. This study provides, in real time, an ultrafast time-resolved detailed description of the significant processes that occur as a result of the interaction of a femtosecond light-pulse with the Cu (111) crystal surface. *Published by AIP Publishing.* [http://dx.doi.org/10.1063/1.4975198]

I. INTRODUCTION

The effect of ultrafast, femtosecond, pulse heating of condensed matter, such as metals and semiconductors, has been associated with a number of fundamental dynamical processes that occur on the femtosecond to picosecond temporal scales. Because the electron heat capacity is typically orders of magnitude lower than that of the lattice, upon femtosecond laser irradiation of a metallic crystal sample, the photon energy is deposited by the photon–electron interaction within the pulse width into the conduction band electrons located within the optical absorption depth (skin depth). The hot electrons equilibrate at a temperature of tens of thousands Kelvin within hundreds of femtoseconds by means of electron–electron interactions, whereas the lattice system remains at room temperature. Within a few picoseconds time interval, after the electron–phonon interaction, the thermal energy is transferred from the electron system to the lattice system through electron–phonon coupling until a thermal equilibrium state is established. Such a two-step non-equilibrium energy transfer process is usually described by the well-known two-temperature model (TTM).[1–5] During the first stage, the sharp temperature gradient of the hot electrons within the optical absorption depth generates a transient elastic stress, blast force,[6] which develops the pressure wave and blast wave, within the laser pulse width. Such a blast wave typically lasts 1–2 ps and propagates at sonic speed within the bulk of the crystal, altering the lattice parameters.[7] The properties of this blast force have been studied in detail theoretically,[8–10] and its effects on the lattice have also been experimentally observed by means of time-resolved x-ray diffraction (XRD).[11,12] In the second

stage, the energy is transferred to the lattice phonons through electron–phonon coupling within a few picoseconds, and a portion of the energy may also be carried into the bulk by ballistic hot electrons, which typically have a mean free path on the order of 100 nm in metals.[12] However, in our case, the ballistic electrons generally account for a very small portion of the heat transferred, which is supported by experimental observations that show that the melting at high pump fluences occurs only within the skin depth of 15 nm. An increase in lattice temperature causes strain and launches acoustic waves that propagate with sonic velocity within the crystal sample. For thin films grown on substrates, the blast waves and acoustic waves are reflected at the substrate, forming a standing wave between the sample surface and the substrate, causing expansion and compression, "breathing motion," of the lattice.[13] Such coherent phonon generation has been detected in ultrafast electron diffraction studies on Al[14] and time-resolved x-ray diffraction of Au.[15]

At large pump fluences, sufficient laser energy is coupled into the lattice through photon–electron, electron–electron, electron–phonon, and phonon–lattice interactions, the crystal temperature reaches the melting point, and the long range lattice order disappears. The time scale of such purely thermal melting of metals is mainly determined by the electron–phonon coupling process that usually takes place within several picoseconds. Ultrafast electron diffraction studies revealed that the melting of 20 nm Al and Au takes 3.5 ps and ~12 ps, respectively,[16,17] whereas ultrafast x-ray diffraction shows that the solid to liquid transition of a 150 nm thick Au crystal occurs in 8 ps.[15] In addition, non-thermal melting was also observed experimentally for semiconductors including Si, GaAs, and InSb, irradiated at fluences that were insufficient to heat them to their melting point.[18–22] This

a)Electronic mail: prentzepis@tamu.edu

non-thermal melting is due to the laser-induced excitation of electrons that alter the interatomic potential and eventually collapse the lattice. Because non-thermal melting does not involve heat transfer, it is expected to occur at a shorter time scale, namely, 1 ps or less. However, depending on the laser fluence,[23] the melting could be the combination of thermal and non-thermal mechanisms. Which mechanism dominates the solid to liquid phase transition for gold[17,24,25] and aluminum[16,26,27] is still debated.

In this study, a 400 nm, 100 fs pulse struck the surface of a 150 nm Cu (111) single crystal and the effect of the pulse on the crystal was monitored by femtosecond Cu K_α x-ray pulses. At low fluence, 10 mJ/cm^2, we measured, in real time, picosecond time heating and the generation of a blast force (contraction of lattice) and coherent phonons. At higher fluence, melting, annealing, mosaic crystal formation, and recrystallization were observed in the actual skin depth of the sample. The experimental data agreed well with our theoretical, TTM, simulations. Monitoring these processes in real time from excitation to tens of picoseconds after excitation, by means of ultrafast time-resolved XRD, we determined the dynamics and mechanism of the processes evolved. For example, the observed picosecond ($\sim$8 ps) melting suggests that the melting in this case is a thermal process.

II. EXPERIMENTAL

The time-resolved x-ray diffraction system has been described in detail in our previous publications.[28] The system includes a femtosecond (fs) laser system that is capable of delivering 100 mJ/pulse, 800 nm, 100 fs laser pulses at a 10 Hz repetition rate, a vacuum chamber for the generation of ultrashort x-ray pulses, a sample holder that provides rotation, 3-dimensional translation, and tilting adjustments, a 2 K $\times$ 2 K x-ray CCD with a pixel size of 13.5 μm $\times$ 13.5 μm and a linear translation stage that precisely control the relative time difference between the arrival of the pump and probe pulses on the crystal. The 800 nm fs laser pulse emitted from the fs laser system was directed onto a beam splitter, with 20% of the pulse being frequency doubled to 400 nm by a Beta-Barium Borate (BBO) crystal, and used to excite the 150 nm Cu (111) single crystal. The remaining 80% of the laser pulse was focused onto a 0.25-mm-diameter moving copper wire, placed in a low vacuum chamber, generating laser-plasma femtosecond Cu K_α x-ray pulses. A 0.3 mm slit placed $\sim$4.5 cm away from the x-ray source collimated the x-ray beam that was transmitted through the 0.1 mm Be window of the x-ray generating chamber. The single crystal Cu (111) sample was placed $\sim$14 cm away from the slit and rotated to a diffraction angle of 21.8°, which corresponds to the diffraction angle of the Cu K_α line. The probe 8.04 keV x-ray pulse contained $\sim$10^6 photons/s at the sample position. The diffraction patterns were acquired by $\sim$8 min integration through the x-ray CCD, which was situated approximately 21 cm from the sample. The relative delay time between the pump laser and probe x-ray pulses was precisely controlled by a linear translation stage. The 400 nm pump beam was focused onto the Cu (111) single crystal to a size of $\sim$2.5 mm $\times$ 1.5 mm with an optical

penetration depth of 15 nm. The 150 nm Cu (111) single crystal was grown on mica at a substrate temperature of 400 °C. Mica is the preferable substrate because it is stable at the 400 °C growing temperature of the single crystal. It is also easily cleavable and a cost-efficient substrate for Cu(111) single crystal growth. The crystal surface was measured by a scanning electron microscope, and its crystal quality was determined by means of CW x-ray diffraction, which confirmed that the sample is a Cu (111) single crystal. However, such films have the usual defects that are found in epitaxial thin films. The reflectivity of the Cu (111) single crystal suggested that 56% of the 400 nm pump beam energy was absorbed by the sample.[29] The diffraction of the probe x-ray pulses is governed by the first order Bragg diffraction law

$$2d \sin \theta = \lambda, \tag{1}$$

where d, θ, and λ are the lattice plane distance, diffraction angle, and wavelength of the probing x-ray pulse, respectively. This equation implies that even small changes of the lattice plane distance can induce measurable shifts of the diffraction angle. Differentiating on both sides of Eq. (1) yields

$$\frac{\Delta d}{d} = -\frac{\Delta \theta}{\tan \theta}. \tag{2}$$

Therefore, the deformation of the lattice plane(s) after laser irradiation is connected with the shift of the diffraction line, which is an experimentally observable parameter. It is worth mentioning that in ultrafast electron diffraction studies,[30] the diffraction angle is typically a hundredth of a degree and $\Delta d/d \approx -\Delta \theta/\theta$ is valid due to the small angle approximation. However, this relation is invalid in time-resolved x-ray diffraction because the diffraction angle is usually large (21.8° for the Cu(111) sample in this paper). Typical x-ray diffraction rocking curves with and without laser excitation are shown in the inset of Figure 1(b). The x-ray CCD array is large enough to record simultaneously the diffraction from both the excited (signal) and non-excited (reference) areas of the sample. Both the signal and reference areas were vertically integrated to obtain their corresponding one dimensional intensity plots and then fitted to a Gaussian function to extract the peak shift and width broadening at each delay time, which provide information regarding lattice spacing change and lattice disorders, respectively. The total intensity at each delay time is obtained by normalizing the integrated x-ray diffraction intensity of the signal area over the reference area to eliminate the pulse-to-pulse fluctuations of the probe x-ray pulse. Then, the normalized total intensities before time zero are averaged and set as the new reference to be used for the normalization of the intensities after time zero.

III. RESULTS AND DISCUSSION

As previously discussed, upon femtosecond laser irradiation, the photon energy is initially absorbed by the free-electrons of the Cu (111) single crystal within the 15 nm optical penetration depth. Owing to the much smaller heat capacity of the electrons compared to the lattice system, the temperature of the electrons is initially very high ($\sim$10^4 K),
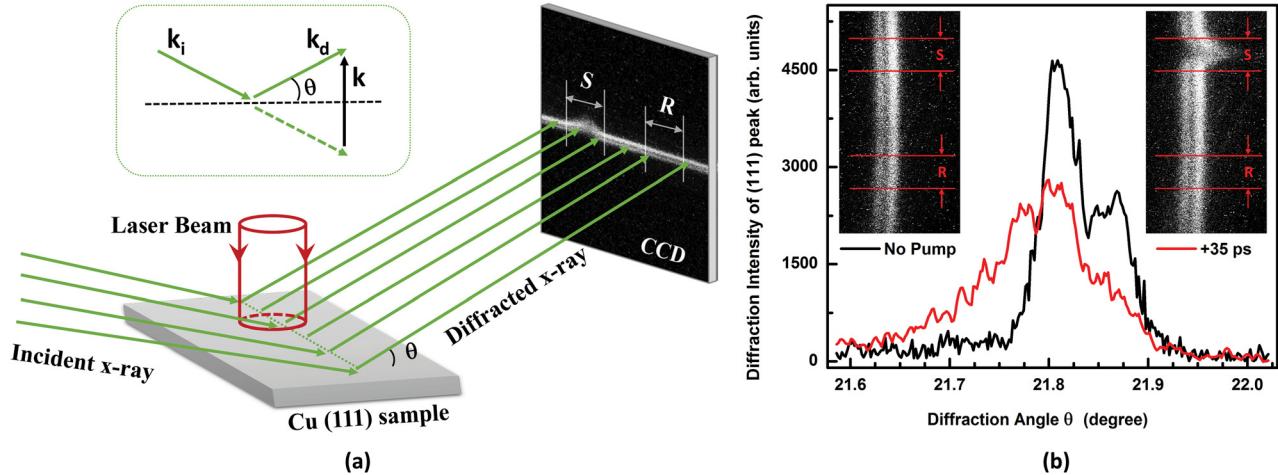
FIG. 1. (a) Geometric relationship of the sample, the detector, probing x-rays, and pumping laser. Inset: the relation between the scattering vector k, incident x-ray wave vector k_i, and diffracted x-ray wave vector k_d. Although the lattice vibrations measured in this study are along the scattering vector, there is no need for the lattice vibration directions or pump laser beam to be strictly aligned with the scattering vector. (b) Rocking curves of the excited areas of the 150 nm Cu (111) sample, at 35 ps delay time and without laser irradiation (no pump). The pump fluence is 17.5 mJ/cm². Inset: the CCD image recorded after 8 min exposure. Diffraction signals from the excited and non-excited areas of the sample are marked as S and R, respectively. The double lines of the diffraction pattern are the $k\alpha_1$ and $k\alpha_2$ diffractions.

whereas the crystal surface remains cold, essentially at room temperature. Then, the non-equilibrium hot electrons formed within the optical penetration depth quickly transfer their energy to the electron system through the electron–electron interaction and the lattice system through electron–phonon coupling, until the entire crystal reaches a thermal equilibrium. The non-equilibrium hot electrons and temperature gradient contribute to the generation of blast force, sonic waves, and thermal evolution at pump fluences below the damage threshold. Increasing the pump photon fluence, the crystal temperature can be raised to the melting point, or above, allowing us to observe and record, in real time, the melting phase transition of the surface layer of the crystal, followed by annealing and recrystallization.

A. Blast force, compression wave, and coherent phonon generation at low laser fluence

The peak shift of the 150 nm Cu (111) x-ray diffraction rocking curve is shown in Figure 2, for pump fluences that vary from 7 mJ/cm² to 12 mJ/cm². It is clear from Figure 2(a) that, after laser excitation, the peak shift is negative for the first few picoseconds and reaches its negative maximum around 3.3 ps. After that, the peak shift moves toward the positive direction and continues to increase, followed by a

damping oscillation that persisted for more than 100 ps. The negative peak shift indicates that the (111) lattice plane distance becomes shortened, a few ps after laser excitation, which suggests contraction of the crystal planes. This can be attributed to the theoretically predicted and experimentally observed compression wave.[6,15] This compressive wave, due to the blast force formed initially on the surface layer of the crystal, propagates through the bulk of the crystal; therefore, the surface layer of the sample is initially denser with a reduced lattice plane distance. As a consequence, the experimental data shown in Figure 2(a) reveal a negative peak shift for the first few picoseconds. The contraction between such excited areas and the cold areas of the crystal occurs before the phonon–phonon interaction and thermalization. Because the laser pulse penetrates only through the few top lattice planes of the sample (15 nm), whereas the x-ray pulse probes the entire 150 nm thickness of the sample, it is expected that the observed x-ray contraction signal accounts for only ~10% of the overall diffraction signal. As can be seen in Figure 2(a), the contraction represented by the shift signal is, proportionally small, around 2×10^{-4}. After the contraction stage, the electron–phonon and the phonon–phonon coupling take place and contribute to the establishment of the thermal equilibrium state for the entire crystal. Therefore, the thermal energy deposited into the skin depth propagates through the
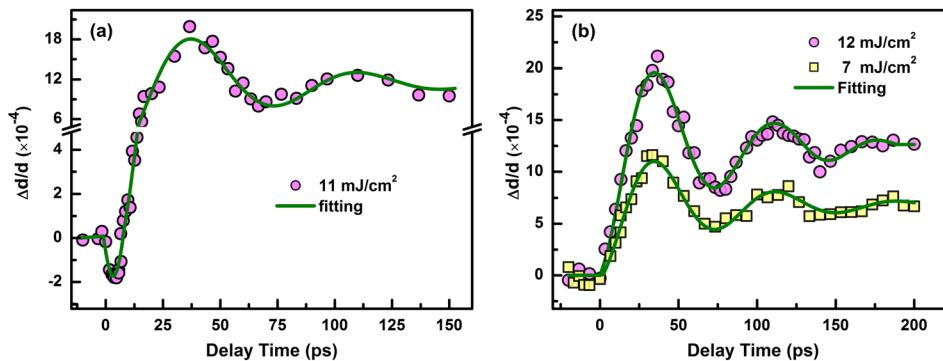

FIG. 2. Peak center shift of the x-ray diffraction rocking curve. (a) Peak shift at a pump fluence of 11 mJ/cm². The contraction of the lattice around the first few picoseconds is due to the blast wave. (b) The peak shift at pump fluences of 7 mJ/cm² and 12 mJ/cm². The contraction is not observed because of the large delay time step, ~14 ps, used during the data acquisition.

bulk and heats the entire depth of the crystal. The elevated temperature of the crystal induces thermal expansion, which was displayed by the increased peak shift of the x-ray diffraction rocking curve, illustrated in Figure 2. In addition to the increased peak shift, several damping oscillations are also observed in the current experiments. Those periodic oscillations, which represent lattice vibration, indicates the generation of coherent phonons.[13,31] Similar lattice vibrations have been observed in time-resolved electron diffraction studies of 20 nm thin Al crystals.[32,33] Previous time-resolved XRD experiments on a 400 nm Ge single crystal also revealed a similar damping oscillation of the lattice planes.[34] Theoretical studies based on the two-temperature model (TTM) and the Fermi-Pasta-Ulam anharmonic chain model have been applied to explain the experimentally observed acoustic oscillations.[35,36] It has been shown in previous time-resolved XRD studies of Au single crystals that the laser fluence does not affect significantly the period of the coherent phonon oscillations.[12] Similar results are found in the present study for the copper crystals, Figure 2(b), for two different pump fluences of 7 mJ/cm² and 12 mJ/cm². The oscillations can be simplified to a one-dimensional standing wave between the crystal surface and the mica substrate. The oscillation period, T, may be calculated using the longitudinal velocity of the acoustic wave v in solid copper

$$T = 2L/v, \tag{3}$$

where L = 150 nm is the thickness of the copper single crystal sample and 4660 m/s is the sound velocity in solid copper. Therefore, the calculated oscillation period T is 64 ps, which agrees with our observation of ~69 ps, average of the two damping periods shown in Figure 2. The damping of those oscillations is attributed to the energy dissipated, mainly, onto the mica substrate. The damping takes about 180 ps, and after that, the peak shift of the x-ray rocking curve remains unchanged up to the longest delay time, 200 ps, in our experiments.

The temperature change in the lattice is associated with the change in the lattice plane distance Δd and therefore the peak shift of the x-ray rocking curve. Designating the thermal expansion coefficient of copper by α, it can be easily shown that

$$\Delta T_l = \frac{1}{\alpha}\frac{\Delta d}{d} = -\frac{1}{\alpha}\frac{\Delta \theta}{\tan \theta}. \tag{4}$$

Assuming a purely thermal process, the temperature change of lattice ΔT_l depends linearly on the laser intensity absorbed by the sample I_{abs}

$$\Delta \theta \propto \Delta T_l \propto I_{abs}. \tag{5}$$

Increasing the pump laser fluence, it is expected that the peak shift of the x-ray rocking curve would increase linearly. This relation is only valid for low pump fluences where the thermal expansion coefficient is a constant and no melting is observed. It should be noted that temperature is defined as a statistic parameter that describes the equilibrium state of a large number of particles. Given the non-equilibrium heating

of the crystal due to the ultrafast energy deposition through femtosecond laser pulse excitation, the lattice temperature being discussed here is the "equivalent temperature," which assumes that temperatures can be defined around each lattice position at a particular time. This is generally used to define the temperature in ultrashort laser pulse–matter interaction studies. This equivalent temperature takes each unit cell as a mini equilibrium system with representative electron and lattice temperatures and uses them to define the temperature of the entire crystal, which is a non-equilibrium system. Increasing the pump laser fluence, from 3.5 mJ/cm² to 17 mJ/cm², the peak shift changed as shown in Figure 3. The two representative peak shifts of each pump fluence are chosen at delay times of 35 ps and 180 ps. At a delay time of 35 ps, the oscillations reach their maximum amplitude, whereas at around 180 ps delay time, the peak shift reaches almost at a plateau. The linear relation indicated by the log-log plot of Figure 3 agrees well with the theoretical analysis of Eq. (5) and also shows that the Cu single crystal heated by the ultrashort laser pulse is a thermal process.

The broadening of the XRD rocking curve vs delay times at two different pump energies is shown in Figure 4(a) where the pump fluence vs broadening, at two representative delay times, 35 ps and 180 ps, is depicted in Figure 4(b). The oscillation period of the broadening is the same as that observed for the peak shift, showing the propagation of sonic waves between the surface layer of the crystal and the substrate. According to previous studies, the broadening due to the blast force and thermal stress depends upon the second order of pump laser intensity and lattice temperature.[8–12,37] Therefore, the relation between the broadening of the rocking curve, $\Delta FWHM$, and the pump laser intensity, I_{abs}, is given by

$$\Delta FWHM \propto (\Delta T_l)^2 \propto I_{abs}^2. \tag{6}$$

As depicted in Figure 4(b), the linear fitting of the log-log plot shows that the broadening at 35 ps and 180 ps changes with slopes of 1.5 and 2.1, respectively. Those slopes agree
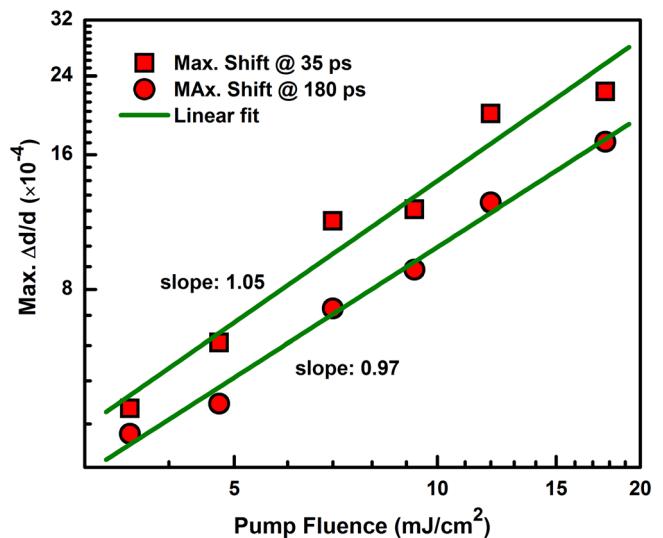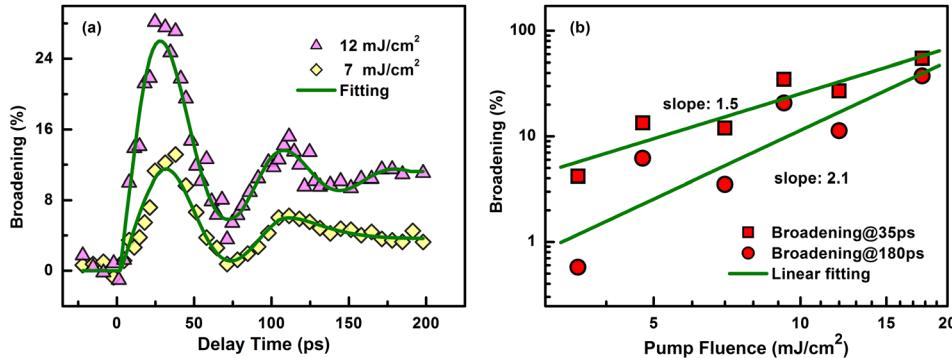

FIG. 3. Energy dependence of the peak shift at two representative delay times, namely, 35 ps and 180 ps. The linear fitting in the log-log plot indicates a linear slope.

FIG. 4. (a) Diffraction line broadening at pump fluences 7 mJ/cm^2 and 12 mJ/cm^2 and (b) pump fluence-dependent broadening of the XRD rocking curve at two representative delay times: 35 ps and 180 ps. The linear fit in the log-log plot shows slopes of 1.5 and 2, which indicates a nonlinear dependence of broadening on the pump fluence.

with the prediction of Eq. (6), which further provides evidence that the broadening caused by the non-thermal expansion and compression of the x-ray rocking curve is due to the stress and tension generated from the blast and sonic waves within the crystal.

B. Melting and annealing of the Cu (111) single crystal at high laser fluence

With the excitation fluence gradually increased to the melting temperature of copper, 1357 K, solid-to-liquid phase transformation is expected to occur on the 15 nm skin depth of the crystal, followed by annealing, mosaic crystal formation, and recrystallization. Time-resolved electron diffraction, x-ray scattering, and optical spectroscopic techniques have been previously utilized to study melting of metals and semiconductors.[38–44] In this study, we observed the solid–liquid and liquid–solid phase transformation and other processes of the Cu (111) single crystal induced by irradiating it with intense 400 nm femtosecond laser pulses. The crystal structure was monitored through the temporal evolution of the XRD intensity. The pump fluence used, ∼58 mJ/cm^2, was insufficient to induce damage to the crystal while intense and energetic enough to trigger melting within the skin depth. As depicted in Figure 5, at negative delay times, before excitation, the XRD signal is in all aspects the same

FIG. 5. The time-dependent intensity change of the x-ray rocking curve. The 150 nm Cu (111) single crystal is irradiated with a 400 nm, 100 fs, ∼58 mJ/cm^2 laser pulse.

as those recorded at room temperature, without laser irradiation. At delay times of ∼8 ps after laser irradiation, a sharp decrease in the XRD intensity of the 150 nm Cu (111) single crystal was observed. After that, the XRD signal intensity begins to increase until ∼40 ps and then it takes more than 80 ps for the diffraction intensity to recover to its original value. Diffraction signals recorded after the crystal is cooled down to room temperature are the same as those obtained at the start of the experiment, without fs pulse excitation, which indicates that the copper crystal remains undamaged throughout the experiment and there is no observable amorphous states within the resolution of our experimental setup. The entire process is attributed to the melting and annealing of the Cu (111) single crystal, which generally consists of three steps: (i) the removal of crystal defects that cause the internal stresses inside the crystal by means of melting or softening; (ii) the growing of grains that introduces new internal stress if the crystal temperature remains high enough to maintain the annealing condition; and (iii) the mosaic crystal formation and recrystallization processes that remove the internal stresses owing to nucleation and growing of new strain-free grains.

The decrease in the XRD intensity, ∼7%, during the first few picoseconds is attributed to melting or atomic disorder of the Cu (111) single crystal. Due to the limited fs light absorption depth, the picosecond disorder process occurs only within the optical skin depth (15 nm for 400 nm pump laser wavelength). However, the femtosecond x-ray pulses penetrate through and probe the entire 150 nm thick copper crystal. As a consequence, only a small portion of approximately 10%, 15 nm skin depth, is expected to be affected by melting. This also suggests that ballistic electrons are few and do not affect the melting process. If a significant amount of the laser energy is carried into the bulk of the sample by ballistic electrons, the entire sample would melt within the first few picoseconds and the total diffraction intensity will decrease by nearly 100%, which means no diffraction signal would be observed. The experimental data presented here also show that the rate of melting is estimated to be $1.5 \times 10^{11} \, s^{-1}$. Given that the electron–phonon interaction and the phonon–lattice interaction are on the order of picoseconds, our experimental data suggest that thermal melting, rather than interatomic potential change due to electronic excitation, is the main mechanism, which agrees with previously published reports.[15] The melting threshold determined in this study only causes reversible recrystallization within the skin depth, which is studied by fs x-ray pulses. Therefore, it is
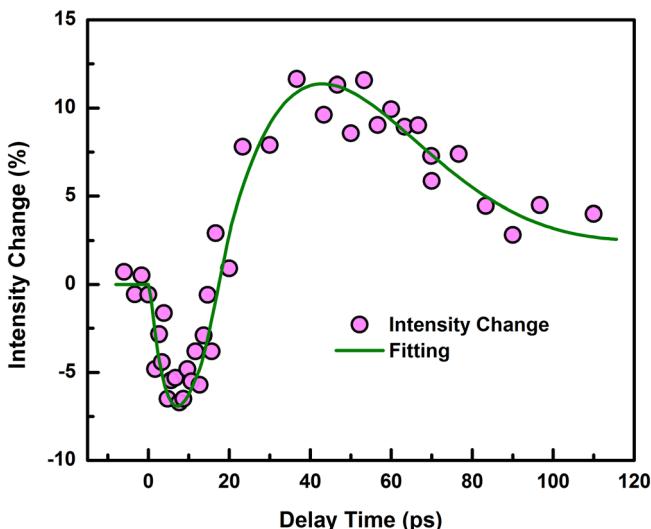
different from the traditional damage threshold measurements performed on bulk materials, which examine the sample surface after laser irradiations by microscopy.

The increase in the XRD intensity from ∼93%, at about 8 ps, to approximately 114%, at 40 ps, after laser excitation is attributed to softening, mosaic crystal formation, and recrystallization. For the laser fluence used for melting, the ∼15 nm surface layer, we expected that only softening of interatomic potential of the inner bulk of the crystal will occur.[45] Considering that the heat capacity of energetic electrons is on the order of 10^6 J/m^{-3} K, the electron temperature within the skin depth is estimated to be 10^4 K during the laser irradiation period. Those hot electrons are quickly equilibrated and transfer their energy to the cold lattice of the skin depth (surface area) by electron-phonon coupling and cause, within picoseconds, the disappearance of long range order, in that area. Meanwhile, the surface area that is at elevated temperatures also transfers energy into the bulk of the Cu (111) crystal through thermal diffusion. As the heat energy is transferred from the skin to the inner bulk of the crystal through the phonon–phonon interaction, the temperature of the surface layer decreases. When the temperature of the surface layer decreases below the melting point, recrystallization occurs. Meanwhile, the heat transferred to the inner crystal area is expected to induce softening. The dynamic of these processes involves both the interior deformation of the crystal and the crystallization of the skin. Grains are microscopic crystals held together through their boundaries where crystals of different orientations meet. During the nucleation, which results from the decreased temperature, the size of the grains increases and the boundaries between grains decrease in number. During the growth of grains, blocks of mosaic crystals are formed with dimensions on the order of 10^{-5} cm, which are estimated to tilt by fractions of a minute of arc with respect to one another. Because the x-ray beam is not ideally collimated but has a small divergence angle of 0.4°, more x-rays within the illumination area will be diffracted by the slightly tilted mosaic crystals. Due to the incoherence of diffraction waves from different mosaic crystal areas, the total XRD intensity is the sum of individual signals from

each mosaic block. Therefore, the observed XRD intensity, at around tens of picoseconds, may exceed the diffraction intensity of the original crystal. During annealing of the crystal, the mosaic crystal "fuses" into a single-orientation (single crystal), which is confirmed by the decrease in the XRD intensity, approaching the value before excitation. The effects of diffraction intensities owing to mosaic crystals formation have been theoretically pioneered by Darwin in the early 1920s[46–48] and also experimentally observed later.[49,50] It is also worthy to note that the dip of the diffraction peak position changes due to the compression wave occurred around 3.3 ps, whereas the melting revealed by the intensity drop is around 8 ps, which provides experimental evidence that the strain revealed by the peak breath is unrelated to the intensity drop caused by lattice collapse. Similar observations have also been reported in ultrafast electron diffraction experiments.[33,51]

The laser heating of the Cu (111) crystal is simulated through the two-temperature model (TTM), and the results are shown in Figure 6. Because the laser irradiation area is much larger than the signal area probed by the x-ray beam, the three-dimensional laser-metal interaction is reduced to one dimension. Therefore, the electron and the lattice temperature at a given depth below the sample surface for a particular delay time can be described by $T_e(z,t)$ and $T_l(z,t)$, respectively. According to TTM and considering the irradiation by the femtosecond laser pulse $S(z,t)$, the evolution of electrons and lattice temperatures are described by two coupled equations

$$C_e \frac{\partial}{\partial t} T_e(z,t) = \frac{\partial}{\partial z}\left(\kappa_e \frac{\partial}{\partial z} T_e(z,t)\right) \\ - g[T_e(z,t) - T_L(z,t)] + S(z,t), \quad (7)$$

$$C_L \frac{\partial}{\partial t} T_L(z,t) = g[T_e(z,t) - T_L(z,t)]. \quad (8)$$

Because the melting occurs only within the optical skin depth, the effect of latent heat is not considered in this calculation. At low pump fluences where the electron temperature is below thousands of Kelvin, it is a valid approximation to
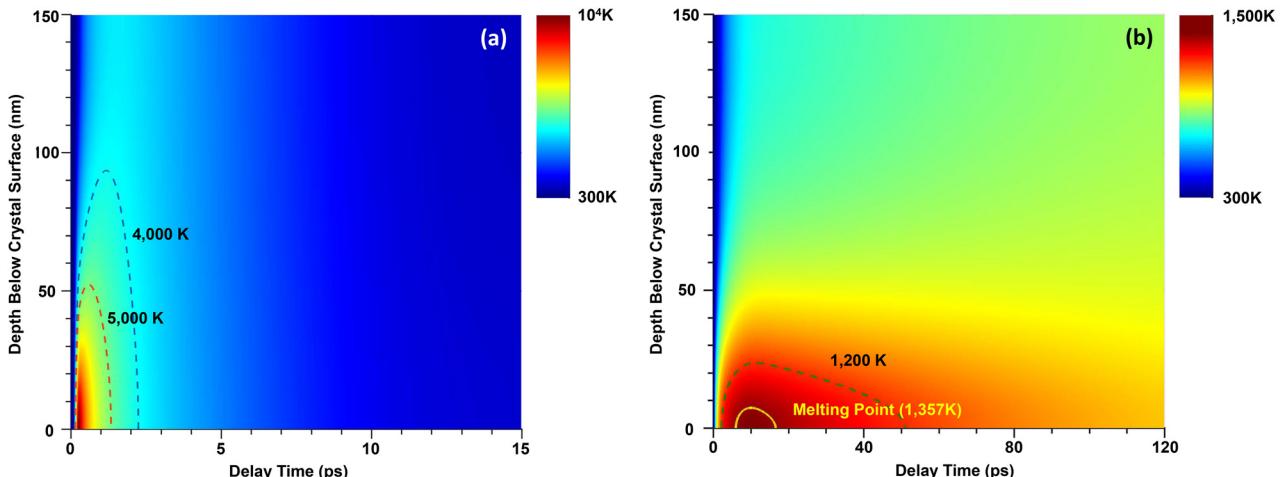

FIG. 6. Spatial-temporal distribution of (a) electrons and (b) lattice temperatures of the Cu (111) single crystal simulated by the two-temperature model. The solid yellow contour curve in (b) indicates the melting point of Cu. A log color scale is used.

assume that the electron–phonon coupling constant, g, is a constant; the electron specific heat capacity C_e is linearly dependent on electron temperature; and the thermal conductivity of electrons, κ_e, is also linearly dependent on the ratio of electrons and lattice temperatures.[52] However, for the high laser fluence used in this experiment, the electron temperature reaches more than 10^4 K. Therefore, the simple temperature dependence of g, C_e, and κ_e is invalid and more accurate modeling of those parameters is required. In this simulation, taking into account the effects of electron–electron and electron–phonon scattering on the electron relaxation time, the electronic thermal conductivity based on the Drude model is used[53–55]

$$\kappa_e = \frac{a_0 T_e}{a_1 T_e^2 + a_2 T_L},\qquad(9)$$

in which $a_0 = 9.7 \times 10^{13}\,\mathrm{W\,m^{-1}\,K^{-2}\,s^{-1}}$, $a_1 = 2.66 \times 10^6\,\mathrm{K^{-2}\,s^{-1}}$, and $a_2 = 2.41 \times 10^{11}\,\mathrm{K^{-1}\,s^{-1}}$. The electron-phonon coupling, g, and electron heat capacity, C_e, are obtained through the fifth order Padé approximations of the data presented in Refs. 55 and 52, respectively

$$g = 1 \times 10^{17}\,\frac{\displaystyle\sum_{n=0}^{5} A_1(n)\left(\frac{T_e}{10^4}\right)^n}{1 + \displaystyle\sum_{n=1}^{5} A_2(n)\left(\frac{T_e}{10^4}\right)^n},\qquad(10)$$

$$C_e = 1 \times 10^5\,\frac{\displaystyle\sum_{n=0}^{5} B_1(n)\left(\frac{T_e}{10^4}\right)^n}{1 + \displaystyle\sum_{n=1}^{5} B_2(n)\left(\frac{T_e}{10^4}\right)^n},\qquad(11)$$

where $A_1(0) = 0.561$, $A_1(1) = -2.263$, $A_1(2) = 9.436$, $A_1(3) = -32.906$, $A_1(4) = 64.683$ and $A_1(5) = 40.393$; $A_2(1) = -3.587$, $A_2(2) = 9.103$, $A_2(3) = -6.258$, $A_2(4) = 8.118$ and $A_2(5) = 6.725$; $B_1(0) = -0.039$, $B_1(1) = 11.995$, $B_1(2) = -76.675$, $B_1(3) = 222.761$, $B_1(4) = -238.574$ and $B_1(5) = 175.460$; $B_2(1) = -5.700$, $B_2(2) = 15.707$, $B_2(3) = -19.342$, $B_2(4) = 13.361$, and $B_2(5) = -0.865$. The TTM Eqs. (7) and (8) were solved using an implicit finite-difference scheme with a grid spacing equal to the lattice plane distance of the Cu (111) single crystal. During the simulation, the heat capacity of the Cu lattice, C_L, was taken as $3.445 \times 10^6\,\mathrm{J\,m^{-3}\,K^{-1}}$. At room temperature, the reduced values for g, C_e, and κ_e are $5.55 \times 10^{16}\,\mathrm{W\,m^{-3}\,K^{-1}}$, $105\,\mathrm{J\,m^{-3}\,K^{-2}}$, and $401\,\mathrm{W\,m^{-1}\,K^{-1}}$.

The two-dimensional plot of the spatial-temporal evolution of electrons and lattice temperatures is given in Figure 6, where the electron temperature is shown to reach its highest value, $\sim 10^4$ K, within 1 ps after laser irradiation, followed by a thermalization within 2 ps. Accompanying the heat transfer from the electron to the lattice, the phonon temperature reaches the melting point in approximately 5 ps. The melting of the surface layer reached the maximum melting depth of 9 nm in around 10 ps. Those results agree with our experimental data, which show that the diffraction intensity dropped

by 7% within 8 ps, indicating that about 10 nm of the surface layer has melted during this time.

IV. CONCLUSION

Direct measurements of transient structure changes in the Cu (111) single crystal illuminated with 400 nm, 100 fs laser pulses have been obtained by means of ultrafast, femtosecond, time-resolved x-ray diffraction. Monitoring the ultrafast evolution of the x-ray diffraction intensity, width, and shift, we have determined directly, in real time, the electron–phonon coupling, the phonon lattice interaction, and the evolution of lattice order, such as the lattice compression due to blast force, breathing motion due to the propagation of acoustic waves, melting, nucleation, mosaic crystal formation, and recrystallization. The long range lattice order disappears within 8 ps, which suggests a thermal melting mechanism. Theoretical simulations, TTM, of the femtosecond pulse interaction with the Cu (111) crystal including electron temperature, lattice temperature, and melting agree well with the experimental data presented.

[1]S. I. Anisimov, B. L. Kapeliovich, and T. L. Perel'man, "Electron emission from metal surfaces exposed to ultrashort laser pulses," Sov. Phys. JETP **39**(2), 375–377 (1974).

[2]M. I. Kaganov, I. M. Lifshitz, and L. V. Tanatarov, "Relaxation between electrons and the crystalline lattice," Sov. Phys. JETP **4**(2), 173–178 (1957).

[3]H. E. Elsayed-Ali *et al.*, "Time-resolved observation of electron-phonon relaxation in copper," Phys. Rev. Lett. **58**(12), 1212 (1987).

[4]J. Hohlfeld *et al.*, "Electron and lattice dynamics following optical excitation of metals," Chem. Phys. **251**(1–3), 237–258 (2000).

[5]T. Juhasz *et al.*, "Direct measurements of the transport of nonequilibrium electrons in gold films with different crystal structures," Phys. Rev. B **48**(20), 15488–15491 (1993).

[6]Y. Gan and J. K. Chen, "Thermomechanical wave propagation in gold films induced by ultrashort laser pulses," Mech. Mater. **42**(4), 491–501 (2010).

[7]L. A. Falkovsky and E. G. Mishchenko, "Electron-lattice kinetics of metals heated by ultrashort laser pulses," J. Exp. Theor. Phys. **88**(1), 84–88 (1999).

[8]L. X. Chen *et al.*, "Capturing a photoexcited molecular structure through time-domain X-ray absorption fine structure," Science **292**(5515), 262–264 (2001).

[9]J. K. Chen, J. E. Beraun, and C. L. Tham, "Ultrafast thermoelasticity for short-pulse laser heating," Int. J. Eng. Sci. **42**(8–9), 793–807 (2004).

[10]J. K. Chen *et al.*, "Short-time thermal effects on thermomechanical response caused by pulsed lasers," J. Thermophys. Heat Transfer **17**(1), 35–42 (2003).

[11]J. Chen *et al.*, "Hot electrons blast wave generated by femtosecond laser pulses on thin Au(1 1 1) crystal, monitored by subpicosecond X-ray diffraction," Chem. Phys. Lett. **419**(4–6), 374–378 (2006).

[12]J. Chen, W.-K. Chen, and P. M. Rentzepis, "Blast wave and contraction in Au(111) thin film induced by femtosecond laser pulses. A time resolved x-ray diffraction study," J. Appl. Phys. **109**(11), 113522–113525 (2011).

[13]M. Nisoli *et al.*, "Coherent acoustic oscillations in metallic nanoparticles generated with femtosecond optical pulses," Phys. Rev. B **55**(20), R13424 (1997).

[14]S. Nie *et al.*, "Measurement of the electronic Grüneisen constant using femtosecond electron diffraction," Phys. Rev. Lett. **96**(2), 025901 (2006).

[15]J. Chen *et al.*, "Time-resolved structural dynamics of thin metal films heated with femtosecond optical pulses," Proc. Natl. Acad. Sci. U.S.A. **108**(47), 18887–18892 (2011).

[16]B. J. Siwick *et al.*, "An atomic-level view of melting using femtosecond electron diffraction," Science **302**(5649), 1382–1385 (2003).

[17]P. Musumeci *et al.*, "Laser-induced melting of a single crystal gold sample by time-resolved ultrafast relativistic electron diffraction," Appl. Phys. Lett. **97**(6), 063502 (2010).

[18]H. W. K. Tom, G. D. Aumiller, and C. H. Brito-Cruz, "Time-resolved study of laser-induced disorder of Si surfaces," Phys. Rev. Lett. **60**(14), 1438–1441 (1988).

[19]M. Harb *et al.*, "Electronically driven structure changes of Si captured by femtosecond electron diffraction," Phys. Rev. Lett. **100**(15), 155504 (2008).

[20]P. Saeta *et al.*, "Ultrafast electronic disordering during femtosecond laser melting of GaAs," Phys. Rev. Lett. **67**(8), 1023–1026 (1991).

[21]A. M. T. Kim *et al.*, "Ultrafast dynamics and phase changes in crystalline and amorphous GaAs," Phys. Rev. B **66**(24), 245203 (2002).

[22]E. S. Zijlstra, J. Walkenhorst, and M. E. Garcia, "Anharmonic noninertial lattice dynamics during ultrafast nonthermal melting of InSb," Phys. Rev. Lett. **101**(13), 135701 (2008).

[23]I. Shumay and U. Höfer, "Phase transformations of an InSb surface induced by strong femtosecond laser pulses," Phys. Rev. B **53**(23), 15878 (1996).

[24]R. Ernstorfer *et al.*, "The formation of warm dense matter: Experimental evidence for electronic bond hardening in gold," Science **323**(5917), 1033–1037 (2009).

[25]T. Ao *et al.*, "Optical properties in nonequilibrium phase transitions," Phys. Rev. Lett. **96**(5), 055001 (2006).

[26]C. Guo *et al.*, "Structural phase transition of aluminum induced by electronic excitation," Phys. Rev. Lett. **84**(19), 4493–4496 (2000).

[27]M. Kandyla, T. Shih, and E. Mazur, "Femtosecond dynamics of the laser-induced solid-to-liquid phase transition in aluminum," Phys. Rev. B **75**(21), 214107 (2007).

[28]J. Chen *et al.*, "Laser induced transient structures in a 150 nm gold crystal," J. Chin. Chem. Soc. **54**(6), 1619–1628 (2007).

[29]H. Ehrenreich and H. R. Philipp, "Optical properties of Ag and Cu," Phys. Rev. **128**(4), 1622–1629 (1962).

[30]R.-Z. Li *et al.*, "Simultaneous investigation of ultrafast structural dynamics and transient electric field by sub-picosecond electron pulses," J. Appl. Phys. **115**(18), 183507 (2014).

[31]A. M. Lindenberg *et al.*, "Time-Resolved X-Ray Diffraction from Coherent Phonons during a Laser-Induced Phase Transition," Phys. Rev. Lett. **84**(1), 111–114 (2000).

[32]H. Park *et al.*, "Direct and real-time probing of both coherent and thermal lattice motions," Solid State Commun. **136**(9–10), 559–563 (2005).

[33]H. Park *et al.*, "Mechanism of coherent acoustic phonon generation under nonequilibrium conditions," Phys. Rev. B **72**(10), 100301 (2005).

[34]A. Cavalleri *et al.*, "Anharmonic lattice dynamics in germanium measured with ultrafast X-ray diffraction," Phys. Rev. Lett. **85**(3), 586 (2000).

[35]J. Tang, "Coherent phonon excitation and linear thermal expansion in structural dynamics and ultrafast electron diffraction of laser-heated metals," J. Chem. Phys. **128**(16), 164702 (2008).

[36]P. Yu, J. Tang, and S.-H. Lin, "Photoinduced structural dynamics in laser-heated nanomaterials of various shapes and sizes," J. Phys. Chem. C **112**(44), 17133–17137 (2008).

[37]J. K. Chen, D. Y. Tzou, and J. E. Beraun, "A semiclassical two-temperature model for ultrafast laser heating," Int. J. Heat Mass Transfer **49**(1–2), 307–316 (2006).

[38]H. E. Elsayed-Ali and P. M. Weber, "Time-resolved surface electron diffraction," in *Time-Resolved Diffraction* (Oxford University Press, 1997), pp. 284–323.

[39]S. Link and M. A. El-Sayed, "Shape and size dependence of radiative, non-radiative and photothermal properties of gold nanocrystals," Int. Rev. Phys. Chem. **19**(3), 409–453 (2000).

[40]J. R. Dwyer *et al.*, "Femtosecond electron diffraction: 'Making the molecular movie,'" Philos. Trans. R. Soc., A **364**(1840), 741–778 (2006).

[41]C.-Y. Ruan *et al.*, "Dynamics of size-selected gold nanoparticles studied by ultrafast electron nanocrystallography," Nano Lett. **7**(5), 1290–1296 (2007).

[42]A. Plech *et al.*, "Laser-induced heating and melting of gold nanoparticles studied by time-resolved x-ray scattering," Phys. Rev. B **70**(19), 195423 (2004).

[43]G. V. Hartland, M. Hu, and J. E. Sader, "Softening of the symmetric breathing mode in gold particles by laser-induced heating," J. Phys. Chem. B **107**(30), 7472–7478 (2003).

[44]S. Link and M. A. El-Sayed, "Spectroscopic determination of the melting energy of a gold nanorod," J. Chem. Phys. **114**(5), 2362–2368 (2001).

[45]D. M. Fritz *et al.*, "Ultrafast bond softening in bismuth: Mapping a solid's interatomic potential with X-rays," Science **315**(5812), 633–636 (2007).

[46]C. Darwin, "XCII. The reflexion of X-rays from imperfect crystals," Philos. Mag. **43**(257), 800–829 (1922).

[47]W. C. Hamilton, "The effect of crystal shape and setting on secondary extinction," Acta Crystallogr. **10**(10), 629–634 (1957).

[48]V. Sears, "Bragg reflection in mosaic crystals. I. General solution of the Darwin equations," Acta Crystallogr., Sect. A: Found. Crystallogr. **53**(1), 35–45 (1997).

[49]G. Bacon and R. Lowde, "Secondary extinction and neutron crystallography," Acta Crystallogr. **1**(6), 303–314 (1948).

[50]J. Wuttke, "Multiple Bragg reflection by a thick mosaic crystal," Acta Crystallogr., Sect. A: Found. Adv. **70**(5), 429–440 (2014).

[51]S. Schäfer, W. Liang, and A. H. Zewail, "Structural dynamics of nanoscale gold by ultrafast electron crystallography," Chem. Phys. Lett. **515**(4–6), 278–282 (2011).

[52]D. S. Ivanov and L. V. Zhigilei, "Combined atomistic-continuum modeling of short-pulse laser melting and disintegration of metal films," Phys. Rev. B **68**(6), 064114 (2003).

[53]C. Wu *et al.*, "Runaway lattice-mismatched interface in an atomistic simulation of femtosecond laser irradiation of Ag film–Cu substrate system," Appl. Phys. A **104**(3), 781–792 (2011).

[54]R. H. Groeneveld, R. Sprik, and A. Lagendijk, "Femtosecond spectroscopy of electron-electron and electron-phonon energy relaxation in Ag and Au," Phys. Rev. B **51**(17), 11433 (1995).

[55]Z. Lin, L. V. Zhigilei, and V. Celli, "Electron-phonon coupling and electron heat capacity of metals under conditions of strong electron-phonon nonequilibrium," Phys. Rev. B **77**(7), 075133 (2008).